


Article

Experimental Investigation of Phase Equilibria in the Co-Ta-Si Ternary System

Cuiping Wang^{1,2}, Xiang Huang^{1,2}, Liangfeng Huang^{1,2}, Mujin Yang^{3,*} , Peng Yang^{1,2}, Yunrui Cui^{1,2}, Jinbin Zhang^{1,2}, Shuiyuan Yang^{1,2} and Xingjun Liu^{1,4,*}

¹ College of Materials and Fujian Provincial Key Laboratory of Materials Genome, Xiamen University, Xiamen 361005, China; wangcp@xmu.edu.cn (C.W.); hx850024430@163.com (X.H.); lfhuang123@163.com (L.H.); 20720191150042@stu.xmu.edu.cn (P.Y.); 13666090301@139.com (Y.C.); jbzhang@xmu.edu.cn (J.Z.); yangshuiyuan@xmu.edu.cn (S.Y.)

² Xiamen Key Laboratory of High Performance Metals and Materials, Xiamen University, Xiamen 361005, China

³ Department of Mechanical and Energy Engineering, Southern University of Science and Technology, Shenzhen 518055, China

⁴ School of Materials Science and Engineering, Institute of Materials Genome & Big Data, Harbin Institute of Technology, Shenzhen 518055, China

* Correspondence: yangmj@sustech.edu.cn (M.Y.); xjliu@hit.edu.cn (X.L.)

Abstract: In this work, two isothermal sections of the Co-Ta-Si ternary system at 900 °C and 1100 °C are constructed in the whole composition range via phase equilibrium determination with the help of electron probe microanalysis (EPMA) and X-ray diffraction (XRD) techniques. Firstly, several reported ternary phases G (Co₁₆Ta₆Si₇), G'' (Co₄TaSi₃), E (CoTaSi), L (Co₃Ta₂Si) and V (Co₄Ta₄Si₇) are all re-confirmed again. The G'' phase is found to be a kind of high-temperature compound, which is unstable at less than 1100 °C. Additionally, the L phase with a large composition range (Co_{32–62}Ta_{26–36}Si_{10–30}) crystallizes with a hexagonal crystal structure (space group: P6₃/mmc, C14), which is the same as that of the binary high-temperature λ₁-Co₂Ta phase. It can be reasonably speculated that the ternary L phase results from the stabilization toward low-temperature of the binary λ₁-Co₂Ta through adding Si. Secondly, the binary CoTa₂ and SiTa₂ phases are found to form a continuous solid solution phase (Co, Si)Ta₂ with a body-centered tetragonal structure. Thirdly, the elemental Si shows a large solid solubility for Co-Ta binary compounds while the Ta and Co are hardly dissolved in Co-Si and Ta-Si binary phases, respectively.

Keywords: Co-based superalloy; phase equilibria; Co-Ta-Si ternary system



Citation: Wang, C.; Huang, X.; Huang, L.; Yang, M.; Yang, P.; Cui, Y.; Zhang, J.; Yang, S.; Liu, X. Experimental Investigation of Phase Equilibria in the Co-Ta-Si Ternary System. *Materials* **2022**, *15*, 3097. <https://doi.org/10.3390/ma15093097>

Academic Editor: Hideki Hosoda

Received: 27 March 2022

Accepted: 22 April 2022

Published: 25 April 2022

Publisher's Note: MDPI stays neutral with regard to jurisdictional claims in published maps and institutional affiliations.



Copyright: © 2022 by the authors. Licensee MDPI, Basel, Switzerland. This article is an open access article distributed under the terms and conditions of the Creative Commons Attribution (CC BY) license (<https://creativecommons.org/licenses/by/4.0/>).

1. Introduction

The γ'-Co₃(Al, W) phase was found to be highly coherent orientation with the γ-Co matrix in the Co-based superalloys similar to the Ni-based superalloys, thus making Co-based superalloys expected to become the next generation of high-temperature structural materials such as aero-engine blades and turbine disk [1,2]. However, the novel Co-based superalloys have severe problems, such as high density and poor stability of γ' phase at high temperatures, which limit their further development [3–5]. Previous studies have shown that the addition of alloying elements such as Ni, Si, Cr, V, Ta, Nb, and Ru can effectively improve the above-mentioned problems and enhance the overall mechanical properties [6–12]. The addition of Ta can improve the stability, volume fraction and solution temperature of the γ' phase, and increase the stress required for the internal slip of the γ' phase to improve the high-temperature mechanical properties of the cobalt-based superalloys [6,9,12]. The addition of Si can improve the oxidation resistance and reduce the density of the Co-based superalloys while maintaining the stability of γ'-phase and high-temperature mechanical properties of the superalloys [10,11]. However, interactions between alloying elements may also cause negative effects. For instance, the excessive

addition of Si and Ta in Co-based superalloys promotes the formation of detrimental topological close-packed (TCP) phases that reduce the strength and ductility [13]. Therefore, theoretical and experimental research on the sub-systems of Co-based superalloy is needed to understand the interrelationship between composition and crystal structure, the related work has achieved considerable achievements [14–21]. Among them, the phase diagram is the theoretical fundamental to guiding the composition design and microstructure control of Co-based superalloys [22,23]. In order to better understand the relationship between the composition and microstructure of the critical Co-based superalloy system Co-Ni-Al-W-Ta-Ti-Hf-Cr-Si [24,25], the phase equilibria of the related sub-system Co-Ta-Si is of great importance.

The Co-Ta-Si ternary system is constituted by three sub-binary systems: Co-Si [26], Co-Ta [27] and Ta-Si [28], as shown in Figure 1. The crystal structure information of each equilibrium phases in the Co-Ta-Si ternary system and three sub-binary systems are shown in Table 1. Firstly, there are five intermediate phases in the Co-Si binary system, namely Co_3Si , $\alpha\text{Co}_2\text{Si}$, $\beta\text{Co}_2\text{Si}$, CoSi and CoSi_2 and six intermediate phases in the Co-Ta binary system: Co_7Ta_2 , Co_6Ta_7 , CoTa_2 , $\lambda_1\text{-Co}_2\text{Ta}$, $\lambda_2\text{-Co}_2\text{Ta}$ and $\lambda_3\text{-Co}_2\text{Ta}$. Among them, the $\lambda_1\text{-Co}_2\text{Ta}$ is a high-temperature MnZn₂-type Laves phase, which decomposes into the CoTa and $\lambda_2\text{-Co}_2\text{Ta}$ phases by an eutectic reaction at 1294 °C. Additionally, the $\lambda_2\text{-Co}_2\text{Ta}$ and $\lambda_3\text{-Co}_2\text{Ta}$ phases are the MnCu₂- and MgNi₂-type Laves phases, respectively. The CoTa_2 Laves phase is a kind of Al₂Cu-type, which is the same as that of the Ta_2Si . Besides, there are six intermediate compounds in the Ta-Si binary system, namely Ta_3Si , Ta_2Si , $\alpha\text{Ta}_5\text{Si}_3$, $\beta\text{Ta}_5\text{Si}_3$, $\gamma\text{Ta}_5\text{Si}_3$, and TaSi_2 . The conversion among $\alpha\text{Ta}_5\text{Si}_3$, $\beta\text{Ta}_5\text{Si}_3$ and $\gamma\text{Ta}_5\text{Si}_3$ are completed through crystal transformation.

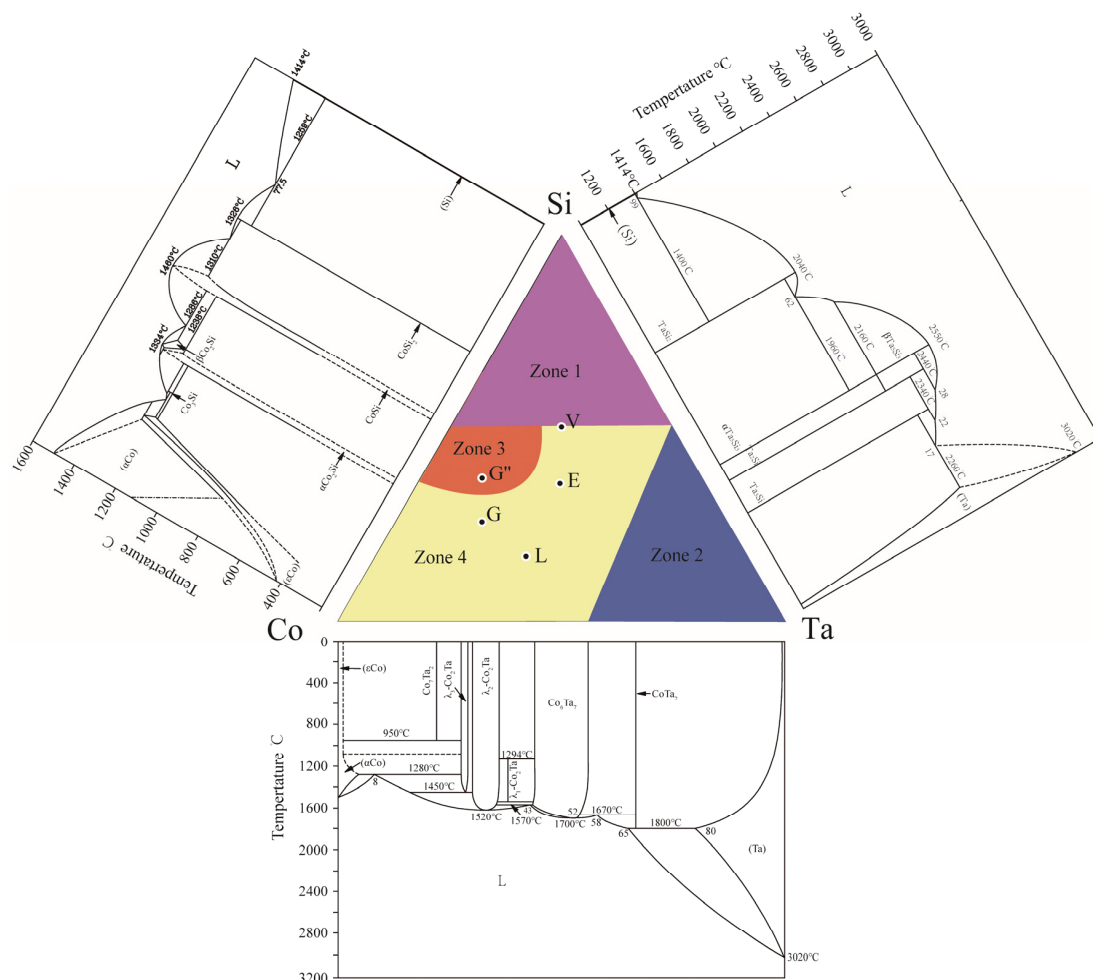


Figure 1. The sub-binary phase diagrams of Co-Si [26], Co-Ta [27] and Ta-Si [28] systems.

Previous studies have reported five ternary compounds in the Co-Ta-Si ternary system: G (Co₁₆Ta₆Si₇) [29], G'' (Co₄TaSi₃) [30,31], L (Co₃Ta₂Si) [32,33], E (CoTaSi) [29,34] and V (Co₄Ta₄Si₇) [34–36]. The G phase was first reported in 1956 by Beattie [37] in A-286 alloy. It is a kind of ternary silicide with a cubic crystal system (space group: Fm $\bar{3}$ m) [38], which was named because it is easy to precipitate at the grain boundaries. Later studies found that there is a special cube-on-cube orientation relationship between the G phase and ferrite, which results in low interfacial energy, and thus makes it a potential strengthening phase of ferritic steel [39]. Additionally, the L phase was detected as a ternary MnZn₂-type Laves phase [32]. Mittal et al. [33] design an alloy with a composition of Co₃Ta₂Si, which detected L and an unknown phase. In addition, the E, G'' and V phases can be treated as stoichiometric compounds and these phases are also detected in Co-Ti-Si [40] and Co-Nb-Si [41] systems.

However, as far as we know, the phase equilibrium of the Co-Ta-Si ternary system has not been reported as far. To better understand the interaction between composition and crystal structure in Co-based superalloys, also to construct the thermodynamic database of the Co-V-Al-Ta-Ti-Ni-Cr-Si multisystem, we devote ourselves to systematically exploring the phase equilibrium relationships in ternary Co-Ta-Si alloys, a sub-system of Co-based superalloys.

Table 1. The stable solid phases in the Co-Ta-Si ternary systems.

System	Phase	Pearson Symbol	Prototype	Space Group	Strukturbericht	Refs.
Co-Si	(α Co)	<i>cF4</i>	Cu	<i>Fm-3m</i>	A1	[26]
	(ϵ Co)	<i>hP2</i>	Mg	<i>P6₃/mmc</i>	A3	[26]
	Co ₃ Si	<i>hP8</i>	Mg ₃ Cd	<i>P6₃/mmc</i>	-	[26]
	α Co ₂ Si	<i>oP12</i>	Co ₂ Si	<i>Pnma</i>	C23	[26]
	β Co ₂ Si	-	-	-	-	[26]
	CoSi	<i>cP8</i>	FeSi	<i>P2₁3</i>	B20	[26]
	CoSi ₂	<i>cF12</i>	CaF ₂	<i>Fm-3m</i>	C1	[26]
	(Si)	<i>cF8</i>	C(diamond)	<i>Fd-3m</i>	A4	[26]
Co-Ta	Co ₇ Ta ₂	<i>hR36</i>	BaPb ₃	<i>R-3m</i>	-	[27]
	λ_1 -Co ₂ Ta	<i>hP12</i>	Zn ₂ Mg	<i>P6₃/mmc</i>	C14	[27]
	λ_2 -Co ₂ Ta	<i>cF24</i>	Cu ₂ Mg	<i>Fd-3m</i>	C15	[27]
	λ_3 -Co ₂ Ta	<i>hP24</i>	MgNi ₂	<i>P6₃/mmc</i>	C36	[27]
	Co ₆ Ta ₇	<i>hR13</i>	Fe ₇ W ₆	<i>R-3m</i>	D8 ₅	[27]
	CoTa ₂	<i>tI12</i>	Al ₂ Cu	<i>I4/mcm</i>	C16	[27]
	(Ta)	<i>cI2</i>	W	<i>Im-3m</i>	A2	[27]
Ta-Si	Ta ₃ Si	<i>tP32</i>	Ti ₃ P	<i>P6₃/mcm</i>	-	[28]
	Ta ₂ Si	<i>tI12</i>	Al ₂ Cu	<i>I4/mcm</i>	C16	[28]
	α Ta ₅ Si ₃	<i>tI32</i>	Cr ₅ B ₃	<i>I4/mcm</i>	D8 ₁	[28]
	β Ta ₅ Si ₃	<i>hP16</i>	Mn ₅ Si ₃	<i>P6₃/mcm</i>	D8 ₈	[28]
	γ Ta ₅ Si ₃	<i>tI32</i>	W ₅ Si ₃	<i>I4/mcm</i>	D8 _m	[28]
	TaSi ₂	<i>hP9</i>	CrSi ₂	<i>P6₂22</i>	C40	[28]
	(Si)	<i>cF8</i>	C(diamond)	<i>Fd-3m</i>	A4	[28]
Co-Ta-Si	CoTaSi (E)	<i>oP12</i>	TiNiSi	<i>Pnma</i>	C23	[34]
	Co ₁₆ Ta ₆ Si ₇ (G)	<i>cF116</i>	Mg ₆ Cu ₁₆ Si ₇	<i>Fm3m</i>	A1	[29]
	Co ₄ TaSi ₃ (G'')	<i>hP168</i>	Y ₁₃ Pd ₄₀ Sn ₃₁	<i>P6/mmm</i>	-	[30]
	Co ₃ Ta ₂ Si (L)	<i>hP12</i>	MgZn ₂	<i>P6₃/mmc</i>	C14	[32]
	Co ₄ Ta ₄ Si ₇ (V)	<i>tI60</i>	Zr ₄ Co ₄ Ge ₇	-	-	[34]

2. Experimental Procedures

High-purity cobalt (>99.9 wt.%, bulk, Beijing Trillion Metals Co., Ltd., Beijing, China), tantalum (>99.9 wt.%, flake, Beijing Trillion Metals Co., Ltd., Beijing, China) and silicon (>99.9 wt.%, block, Beijing Trillion Metals Co., Ltd., Beijing, China) were adopted as starting materials. The samples were prepared by arc-melting using a water-cooled copper crucible with a non-consumable tungsten electrode under the high purity Ar atmosphere (DHL-1250,

Sky Technology Development Co, Ltd., Shenyang, China). The weight of each sample was about 20 g and they were arc-melted at least five times to achieve the compositional uniformity. The overall weight loss after arc-melting was no more than 0.5 wt.%. Then, these samples were sealed in capsules via backfilling with Ar and annealed at 900 °C and 1100 °C, respectively. Considering the high melting point for the elemental Ta, the time of annealing was set as 90 days for 900 °C and 60 days for 1100 °C, respectively. To prevent contamination of samples, the capsules were inserted with Ti scrap and the samples were wrapped with a Ta sheet. After reaching the preset annealing time, the samples were quenched into ice water and prepared by standard metallographic methods.

The equilibrium composition of each phase was investigated by EPMA (electron probe microanalyzer) (JAX-8100R, JEOL, Tokyo, Japan) with WDS (wavelength dispersive X-ray spectroscopy) and BSE (backscattered electrons). Crystal structure analysis was carried out through XRD (X-ray diffractometer) (D8 Advance, Bruker, Karlsruhe, Germany) using Cu K α radiation at 40.0 kV and 40 mA, and the data were collected in the range of 2 θ from 10° to 90° at a step size of 0.0167°.

3. Results and Discussion

3.1. Microstructure and Phase Equilibrium

In Figure 1, the Co-Ta-Si ternary system is divided into four regions (zone 1–4), phase equilibrium from each region is carefully discussed below. The following composition of each phase and alloy is described by the atomic ratio (at.%). The representative micrograph images and corresponding XRD indexing results are given below to indicate the phase equilibria relationship of the alloy. The nominal composition, annealing time and equilibrium composition of each phase measured by WDS are all listed in Tables 2 and 3.

3.1.1. Equilibria at Zone 1

Zone 1 mainly contains the phase equilibria at the Si-rich corner (Si > 50 at.%). For the Co₃₄Ta₂₆Si₄₀ alloy that was annealed at 1100 °C, a distinct three-phase equilibrium of E + V + CoSi was observed in Figure 2a and their crystal structures could be confirmed by the corresponding XRD pattern in Figure 3a. As shown in Figure 2b, the Co₂₆Ta₇Si₆₇ alloy is located in a three-phase equilibria region after being annealed at 1100 °C. The white and light gray phases correspond to the TaSi₂ and CoSi₂ phases, respectively, while the dark gray phase is presumed to be the solid solution phase of Si (signed as (Si)). The corresponding XRD pattern indexing result in Figure 3b further confirmed this speculation.

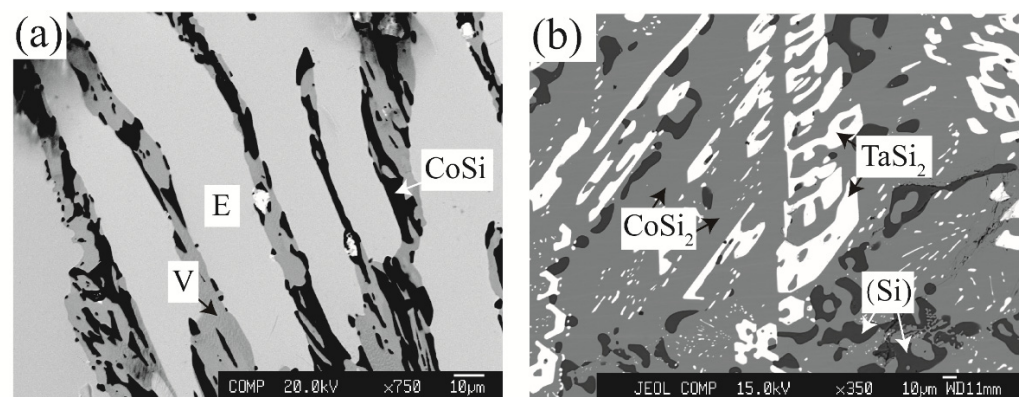


Figure 2. Typical ternary micrograph images obtained of (a) Co₃₄Ta₂₆Si₄₀ alloy annealed at 1100 °C for 60 days and (b) Co₂₆Ta₇Si₆₇ alloy annealed at 1100 °C for 60 days.

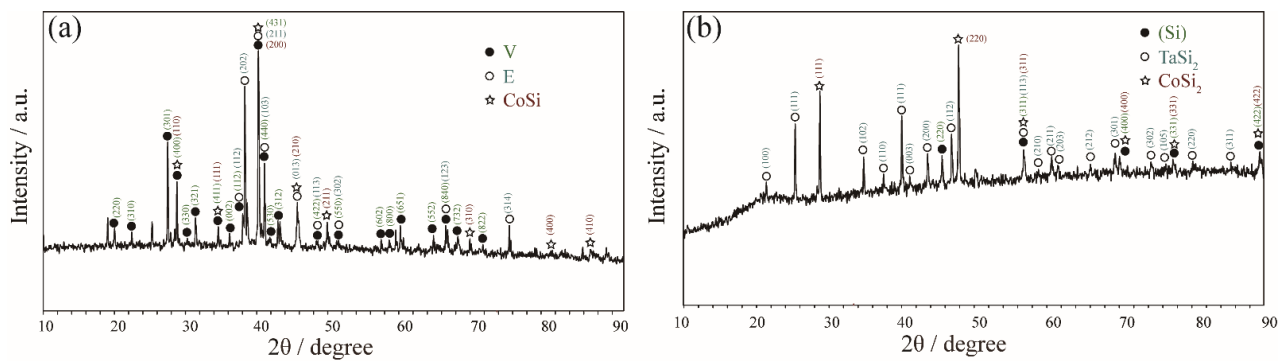


Figure 3. XRD patterns obtained of (a) $\text{Co}_{34}\text{Ta}_{26}\text{Si}_{40}$ alloy annealed at 1100 °C for 60 days and (b) $\text{Co}_{26}\text{Ta}_7\text{Si}_{67}$ alloy annealed at 1100 °C for 60 days.

Table 2. Equilibrium compositions of the Co-Ta-Si ternary system at 900 °C determined in the present work.

Alloy (at.%)	Annealed Time	Phase Equilibria		Composition (at.%)					
		Phase 1/Phase 2/Phase 3	Phase 1		Phase 2		Phase 3		
			Ta	Si	Ta	Si	Ta	Si	
$\text{Co}_{10}\text{Ta}_{10}\text{Si}_{80}$	90 days	$\text{TaSi}_2 / \text{CoSi}_2 / (\text{Si})$	30.3	68.6	0.1	70.3	0.1	99.7	
$\text{Co}_{33}\text{Ta}_{14}\text{Si}_{53}$	90 days	V / CoSi	24.8	48.4	0.1	51.6			
$\text{Co}_{30}\text{Ta}_{43}\text{Si}_{27}$	90 days	$(\text{Co}, \text{Si})\text{Ta}_2 / \lambda_1\text{-Co}_2\text{Ta}$	62.6	30.8	32.2	29.5			
$\text{Co}_{54}\text{Ta}_{28}\text{Si}_{18}$	90 days	$\lambda_1\text{-Co}_2\text{Ta} / \text{G}$	28.2	18.9	19.2	25.1			
$\text{Co}_{16}\text{Ta}_{18}\text{Si}_{66}$	90 days	$\text{TaSi}_2 / \text{CoSi} / \text{CoSi}_2$	30.4	67.8	0.2	51.8	0.2	67.2	
$\text{Co}_{22}\text{Ta}_{27}\text{Si}_{51}$	90 days	$\text{TaSi}_2 / \text{V} / \text{CoSi}$	30.6	67.8	25.3	48.2	0.5	51.6	
$\text{Co}_{27}\text{Ta}_{60}\text{Si}_{13}$	90 days	$(\text{Co}, \text{Si})\text{Ta}_2 / \text{Co}_6\text{Ta}_7$	63.7	22.8	49.6	6.7			
$\text{Co}_{34}\text{Ta}_{26}\text{Si}_{40}$	90 days	$\text{E} / \text{V} / \text{CoSi}$	31.6	34.8	22.7	46.5	0.2	50.5	
$\text{Co}_{25}\text{Ta}_{38}\text{Si}_{37}$	90 days	$\alpha\text{Ta}_5\text{Si}_3 / \text{E} / \text{V}$	58.4	39.0	32.1	35.2	25.2	48.1	
$\text{Co}_{64.5}\text{Ta}_{22.5}\text{Si}_{13}$	90 days	$\lambda_3\text{-Co}_2\text{Ta} / \text{G}$	23.5	11.5	19.9	25.4			
$\text{Co}_{36}\text{Ta}_{54}\text{Si}_{10}$	90 days	$(\text{Co}, \text{Si})\text{Ta}_2 / \text{Co}_6\text{Ta}_7$	64.0	20.6	49.7	9.2			
$\text{Co}_2\text{Ta}_{75}\text{Si}_{23}$	90 days	$(\text{Ta}) / (\text{Co}, \text{Si})\text{Ta}_2 / \text{Ta}_3\text{Si}$	92.3	5.4	63.8	28.6	71.0	28.6	
$\text{Co}_{26}\text{Ta}_7\text{Si}_{67}$	90 days	$\text{CoSi}_2 / \text{TaSi}_2$	0.1	67.5	29.5	67.1			
$\text{Co}_{46}\text{Ta}_{13}\text{Si}_{41}$	90 days	G / CoSi	18.2	25.8	0.1	51.2			
$\text{Co}_{58}\text{Ta}_{10}\text{Si}_{32}$	90 days	$\text{Co}_2\text{Si} / \text{CoSi} / \text{G}$	0.1	34.6	0.1	50.6	18.0	26.2	
$\text{Co}_{48}\text{Ta}_{22}\text{Si}_{30}$	90 days	$\text{E} / \text{G} / \text{CoSi}$	30.2	35.1	18.3	26.1	0.1	51.1	
$\text{Co}_{36}\text{Ta}_{33}\text{Si}_{31}$	90 days	$\text{E} / \lambda_1\text{-Co}_2\text{Ta}$	30.9	35.2	31.1	30.9			
$\text{Co}_{59.5}\text{Ta}_{22.5}\text{Si}_{18}$	90 days	$\lambda_3\text{-Co}_2\text{Ta} / \text{G}$	22.1	11.0	18.6	24.6			
$\text{Co}_{59}\text{Ta}_{31}\text{Si}_{10}$	90 days	$\lambda_1\text{-Co}_2\text{Ta} / \lambda_2\text{-Co}_2\text{Ta}$	29.7	13.0	28.8	8.5			
$\text{Co}_{11}\text{Ta}_{75}\text{Si}_{14}$	90 days	$(\text{Ta}) / (\text{Co}, \text{Si})\text{Ta}_2$	91.2	3.0	63.7	28.1			
$\text{Co}_{38}\text{Ta}_{58}\text{Si}_4$	90 days	$\text{Co}_6\text{Ta}_7 / (\text{Co}, \text{Si})\text{Ta}_2$	63.3	12.4	52.1	5.9			
$\text{Co}_{25}\text{Ta}_{33}\text{Si}_{42}$	90 days	$\alpha\text{Ta}_5\text{Si}_3 / \text{E} / \text{V}$	57.2	39.6	32.4	35.6	24.4	48.9	
$\text{Co}_{24}\text{Ta}_{44}\text{Si}_{31}$	90 days	$\alpha\text{Ta}_5\text{Si}_3 / \text{E}$	58.1	39.4	31.6	34.8			
$\text{Co}_{65}\text{Ta}_{27}\text{Si}_8$	90 days	$\text{G} / \lambda_3\text{-Co}_2\text{Ta}$	19.1	24.1	25.3	9.2			
$\text{Co}_{56}\text{Ta}_9\text{Si}_{35}$	90 days	$\text{G} / \alpha\text{Co}_2\text{Si} / \text{CoSi}$	19.0	25.0	0.4	33.6	0.3	49.2	
$\text{Co}_{44}\text{Ta}_{25}\text{Si}_{31}$	90 days	$\text{E} / \text{G} / \text{CoSi}$	30.7	33.6	19.3	24.6	0.7	47.4	
$\text{Co}_{10}\text{Ta}_{59}\text{Si}_{31}$	90 days	$\alpha\text{Ta}_5\text{Si}_3 / \text{E} / (\text{Co}, \text{Si})\text{Ta}_2$	58.8	39.4	32.0	29.7	63.4	33.2	
$\text{Co}_{61}\text{Ta}_{11}\text{Si}_{28}$	90 days	$\text{G} / \alpha\text{Co}_2\text{Si}$	17.7	24.8	0.1	32.6			
$\text{Co}_{70}\text{Ta}_9\text{Si}_{21}$	90 days	$\text{G} / (\epsilon\text{Co}) / \alpha\text{Co}_2\text{Si}$	57.7	24.3	0.1	14.4	0.2	29.7	
$\text{Co}_{37}\text{Ta}_{42}\text{Si}_{21}$	90 days	$(\text{Co}, \text{Si})\text{Ta}_2 / \lambda_1\text{-Co}_2\text{Ta}$	62.0	24.7	44.3	22.2			
$\text{Co}_{71}\text{Ta}_{13}\text{Si}_{16}$	90 days	$\text{G} / (\alpha\text{Co})$	18.8	24.4	0.5	6.7			
$\text{Co}_{78}\text{Ta}_{10}\text{Si}_{12}$	90 days	$\lambda_3\text{-Co}_2\text{Ta} / \text{G} / (\alpha\text{Co})$	20.6	8.5	18.7	23.7	0.7	4.0	
$\text{Co}_{51}\text{Ta}_{37}\text{Si}_{12}$	90 days	$\text{Co}_6\text{Ta}_7 / \lambda_1\text{-Co}_2\text{Ta}$	46.5	6.2	32.4	16.2			
$\text{Co}_{41}\text{Ta}_{47}\text{Si}_{12}$	90 days	$(\text{Co}, \text{Si})\text{Ta}_2 / \text{Co}_6\text{Ta}_7 / \lambda_1\text{-Co}_2\text{Ta}$	62.9	22.3	47.6	8.9	36.8	13.5	
$\text{Co}_{78}\text{Ta}_{17}\text{Si}_5$	90 days	$\lambda_3\text{-Co}_2\text{Ta} / (\alpha\text{Co})$	21.0	6.4	0.9	1.9			
$\text{Co}_{57}\text{Ta}_{38}\text{Si}_5$	90 days	$\text{Co}_6\text{Ta}_7 / \lambda_2\text{-Co}_2\text{Ta}$	43.2	4.1	35.5	6.1			
$\text{Co}_{27}\text{Ta}_{68}\text{Si}_5$	90 days	$(\text{Ta}) / (\text{Co}, \text{Si})\text{Ta}_2$	91.7	2.9	63.5	6.2			

Table 3. Equilibrium compositions of the Co-Ta-Si ternary system at 1100 °C determined in the present work.

Alloy (at.%)	Annealed Time	Phase Equilibria	Composition (at.%)					
		Phase 1/Phase 2/Phase 3	Phase 1		Phase 2		Phase 3	
			Ta	Si	Ta	Si	Ta	Si
Co ₁₀ Ta ₁₀ Si ₈₀	60 days	TaSi ₂ / CoSi ₂ / (Si)	31.0	67.3	0.7	68.0	0.1	99.0
Co ₃₃ Ta ₁₄ Si ₅₃	60 days	V / CoSi	25.4	48.2	0.1	50.9		
Co ₁₀ Ta ₃₈ Si ₅₂	60 days	TaSi ₂ / αTa ₅ Si ₃ / V	31.4	68.1	58.5	39.3	25.6	48.8
Co ₄₆ Ta ₂₈ Si ₂₆	60 days	E / G	30.8	34.8	19.7	25.5		
Co ₃₀ Ta ₄₃ Si ₂₇	60 days	(Co, Si)Ta ₂ / λ ₁ -Co ₂ Ta	63.6	30.3	32.9	26.4		
Co ₅₄ Ta ₂₈ Si ₁₈	60 days	λ ₁ -Co ₂ Ta / G	28.2	19.5	20.1	25.4		
Co ₁₆ Ta ₁₈ Si ₆₆	60 days	CoSi / TaSi ₂ / V	30.8	67.6	0.1	51.8	24.5	48.4
Co ₂₂ Ta ₂₇ Si ₅₁	60 days	TaSi ₂ / V	31.4	68.4	25.3	48.9		
Co ₂₇ Ta ₆₀ Si ₁₃	60 days	(Co, Si)Ta ₂ / Co ₆ Ta ₇	63.8	21.1	50.7	7.5		
Co ₃₅ Ta ₅ Si ₆₀	60 days	V / CoSi	23.8	48.6	0.1	51.2		
Co ₃₄ Ta ₂₆ Si ₄₀	60 days	E / V / CoSi	31.8	35.4	25.2	46.8	0.1	51.9
Co ₂₅ Ta ₃₈ Si ₃₇	60 days	E / αTa ₅ Si ₃ / V	57.7	39.6	32.0	35.6	25.7	48.3
Co _{64.5} Ta _{22.5} Si ₁₃	60 days	λ ₃ -Co ₂ Ta / G	22.1	12.6	19.5	23.8		
Co ₂ Ta ₇₅ Si ₂₃	60 days	Ta / (Co, Si)Ta ₂ / Ta ₃ Si	94.8	4.0	64.0	30.0	27.9	71.6
Co ₂₆ Ta ₇ Si ₆₇	60 days	TaSi ₂ / CoSi ₂ / (Si)	30.4	68.1	0.1	67.8	0.1	99.5
Co ₄₆ Ta ₁₃ Si ₄₁	60 days	E / G'' / CoSi	30.2	35.0	13.0	37.4	0.1	50.5
Co ₅₈ Ta ₁₀ Si ₃₂	60 days	αCo ₂ Si / G / G''	0.1	34.7	18.6	25.8	13.6	37.1
Co ₄₈ Ta ₂₂ Si ₃₀	60 days	G / G'' / E	18.7	25.9	13.4	37.3	30.7	34.8
Co ₃₆ Ta ₃₃ Si ₃₁	60 days	E / λ ₁ -Co ₂ Ta	30.7	35.4	30.5	26.8		
Co _{59.5} Ta _{22.5} Si ₁₈	60 days	G / λ ₃ -Co ₂ Ta	18.8	25.1	24.2	15.3		
Co ₅₉ Ta ₃₁ Si ₁₀	60 days	λ ₁ -Co ₂ Ta	28.7	11.3				
Co ₁₁ Ta ₇₅ Si ₁₄	60 days	(Ta) / (Co, Si)Ta ₂	95.0	3.1	63.3	27.9		
Co ₃₈ Ta ₅₈ Si ₄	60 days	Co ₆ Ta ₇ / (Co, Si)Ta ₂	63.5	12.0	52.1	3.4		
Co ₂₅ Ta ₃₃ Si ₄₂	60 days	E / V	31.4	35.9	24.6	48.8		
Co ₂₄ Ta ₄₄ Si ₃₁	60 days	αTa ₅ Si ₃ / E	58.6	39.4	30.8	35.5		
Co ₆₅ Ta ₂₇ Si ₈	60 days	λ ₃ -Co ₂ Ta	25.1	9.1				
Co ₄₂ Ta ₁₅ Si ₄₃	60 days	CoSi / E	0.3	50.8	30.0	35.0		
Co ₂₆ Ta ₃₃ Si ₄₁	60 days	V / E	24.9	48.5	31.3	35.1		
Co ₅₆ Ta ₉ Si ₃₅	60 days	G'' / αCo ₂ Si / CoSi	13.6	36.5	0.1	33.9	0.1	49.3
Co ₄₄ Ta ₂₅ Si ₃₁	60 days	G / G''	18.9	25.6	13.9	36.4		
Co ₁₀ Ta ₅₉ Si ₃₁	60 days	αTa ₅ Si ₃ / Ta ₂ Si / E	58.7	39.1	63.4	34.1	32.9	34.4
Co ₆₁ Ta ₁₁ Si ₂₈	60 days	G / αCo ₂ Si	18.1	24.9	0.2	32.7		
Co ₇₀ Ta ₉ Si ₂₁	60 days	G / (εCo) / αCo ₂ Si	17.9	24.6	0.2	17.4	0.1	32.0
Co ₅₄ Ta ₂₅ Si ₂₁	60 days	λ ₁ -Co ₂ Ta / G	26.8	18.5	19.2	25.6		
Co ₅₄ Ta ₂₅ Si ₂₁	60 days	λ ₁ -Co ₂ Ta	31.2	24.1				
Co ₃₇ Ta ₄₂ Si ₂₁	60 days	(Co, Si)Ta ₂ / λ ₁ -Co ₂ Ta	62.4	26.6	32.5	23.5		
Co ₂₆ Ta ₅₃ Si ₂₁	60 days	(Co, Si)Ta ₂ / λ ₁ -Co ₂ Ta	62.7	26.9	33.9	19.9		
Co ₆₀ Ta ₂₄ Si ₁₆	60 days	λ ₃ -Co ₂ Ta / G	21.3	13.9	18.9	24.5		
Co ₇₈ Ta ₁₀ Si ₁₂	60 days	λ ₃ -Co ₂ Ta / G / (αCo)	20.6	13.8	18.8	24.2	1.3	8.9
Co ₅₁ Ta ₃₇ Si ₁₂	60 days	Co ₆ Ta ₇ / λ ₁ -Co ₂ Ta	45.8	5.5	32.6	10.9		
Co ₄₁ Ta ₄₇ Si ₁₂	60 days	(Co, Si)Ta ₂ / Co ₆ Ta ₇ / λ ₁ -Co ₂ Ta	62.6	21.5	45.9	10.1	33.6	16.5
Co ₂₁ Ta ₆₇ Si ₁₂	60 days	(Co, Si)Ta ₂ / (Ta)	94.1	3.0	63.6	24.5		
Co ₇₈ Ta ₁₇ Si ₅	60 days	λ ₃ -Co ₂ Ta / (αCo)	22.4	7.1	2.6	3.5		
Co ₅₇ Ta ₃₈ Si ₅	60 days	Co ₆ Ta ₇ / λ ₂ -Co ₂ Ta	45.3	3.6	32.5	6.8		

3.1.2. Equilibria at Zone 2

Zone 2 corresponds to the phase equilibria at the Ta-rich corner (Ta > 50 at.%). In Figure 4a, a two-phase equilibrium of (Co, Si)Ta₂ (white) + λ₁-Co₂Ta (black) was confirmed in the Co₃₀Ta₄₃Si₂₇ alloy quenching from 1100 °C based on the support of the corresponding X-ray diffraction pattern in Figure 5. As shown in Figure 4b, the Co₁₁Ta₇₅Si₁₄ alloy formed a two-phase equilibrium microstructure of (Ta) + (Co, Si)Ta₂ after being annealed at 900 °C.

Figure 4c depicts the three-phase equilibrium of $(\text{Co, Si})\text{Ta}_2$ (white) + Co_6Ta_7 (grey) + $\lambda_1\text{-Co}_2\text{Ta}$ (black) in $\text{Co}_{41}\text{Ta}_{47}\text{Si}_{12}$ alloy after being annealed at 900°C .

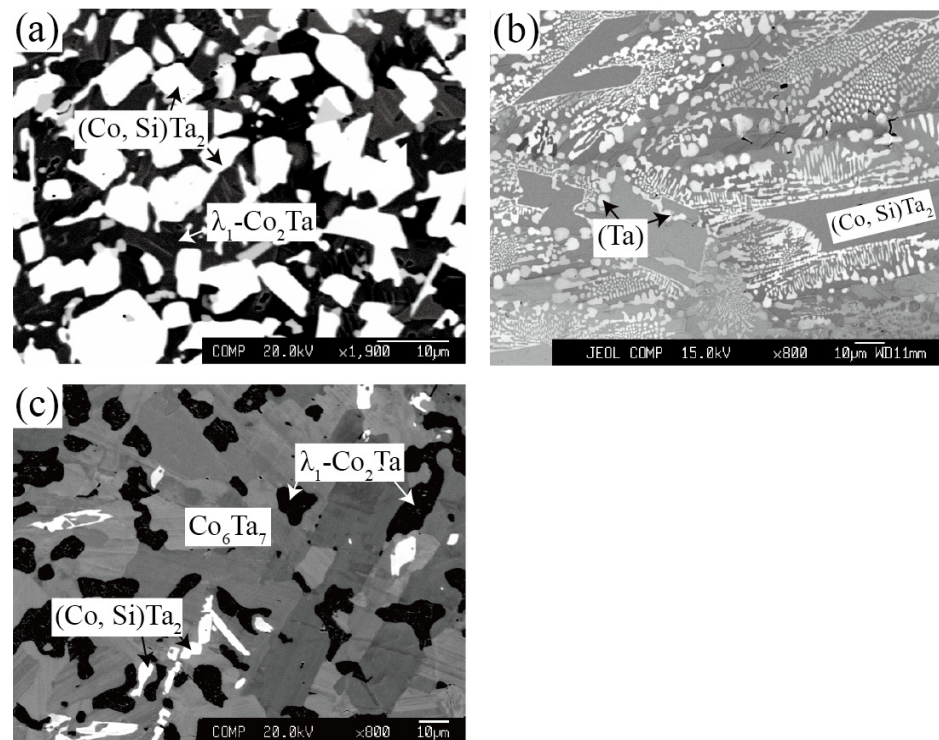


Figure 4. Typical ternary micrograph images obtained of (a) $\text{Co}_{30}\text{Ta}_{43}\text{Si}_{27}$ alloy annealed at 1100°C for 60 days; (b) $\text{Co}_{11}\text{Ta}_{75}\text{Si}_{14}$ alloy annealed at 900°C for 90 days and (c) $\text{Co}_{41}\text{Ta}_{47}\text{Si}_{12}$ alloy annealed at 900°C for 90 days.

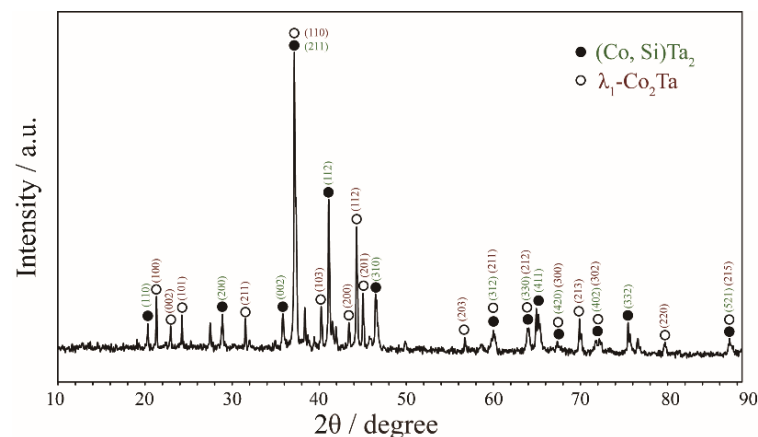


Figure 5. XRD patterns obtained of $\text{Co}_{30}\text{Ta}_{43}\text{Si}_{27}$ alloy annealed at 1100°C for 60 days.

Compositional analysis of the $\text{Co}_{30}\text{Ta}_{43}\text{Si}_{27}$, $\text{Co}_{27}\text{Ta}_{60}\text{Si}_{13}$, $\text{Co}_{36}\text{Ta}_{54}\text{Si}_{10}$, $\text{Co}_2\text{Ta}_{75}\text{Si}_{23}$, $\text{Co}_{11}\text{Ta}_{75}\text{Si}_{14}$, $\text{Co}_{38}\text{Ta}_{58}\text{Si}_4$, $\text{Co}_{10}\text{Ta}_{59}\text{Si}_{31}$, $\text{Co}_{37}\text{Ta}_{42}\text{Si}_{21}$, $\text{Co}_{41}\text{Ta}_{47}\text{Si}_{12}$, $\text{Co}_{27}\text{Ta}_{68}\text{Si}_5$ and $\text{Co}_{26}\text{Ta}_{53}\text{Si}_{21}$ alloys indicate that these alloys contain a phase with about 63 at.% Ta after being annealed at 900°C and 1100°C . The X-ray diffraction analysis results of these alloys strongly suggest that the binary Al_2Cu -type CoTa_2 and Ta_2Si phases form a continuous solid solution phase $(\text{Co, Si})\text{Ta}_2$. As far as we know, it is the first time to discover the infinite mutual solubility between CoTa_2 and Ta_2Si phases. Similarly, the phenomenon of Ni and Si can be entirely substituted by each other in Al_2Cu -type compounds was also found in the Ni-Ta-Si ternary system [42].

3.1.3. Equilibria at Zone 3

Zone 3 mainly discusses the phase equilibria around G'' phase. The alloy $\text{Co}_{46}\text{Ta}_{13}\text{Si}_{41}$, $\text{Co}_{58}\text{Ta}_{10}\text{Si}_{32}$ and $\text{Co}_{48}\text{Ta}_{22}\text{Si}_{30}$ were designed to explore the existence of the G'' phase. For $\text{Co}_{46}\text{Ta}_{13}\text{Si}_{41}$ and $\text{Co}_{58}\text{Ta}_{10}\text{Si}_{32}$ alloys that being annealed at $1100\text{ }^\circ\text{C}$, two three-phase equilibrium $\text{CoSi} + \text{E} + G''$ and $\alpha\text{Co}_2\text{Si} + \text{G} + G''$ were detected as shown in Figure 6a,b. The corresponding XRD patterns in Figure 7a,b indicate that the diffraction peaks belonging to the phases (CoSi , E , $\alpha\text{Co}_2\text{Si}$ and G) are in good agreement with the standard patterns. However, the diffraction peak of the G'' phase was not interpreted due to the lack of crystallographic information. For the $\text{Co}_{48}\text{Ta}_{22}\text{Si}_{30}$ alloy annealed at $1100\text{ }^\circ\text{C}$, a clearly three-phase equilibria $\text{E} + \text{G} + G''$ (white) + G (light gray) + G'' (dark gray) was detected, as shown in Figure 6c. However, the EMPA micrographs and WDS analysis of the same alloy (see Figure 6d) quenching from $900\text{ }^\circ\text{C}$ show that it is a three-phase of $\text{E} + \text{G} + \text{CoSi}$. This result implies that the G'' phase is a high-temperature compound, which is not stable at $900\text{ }^\circ\text{C}$.

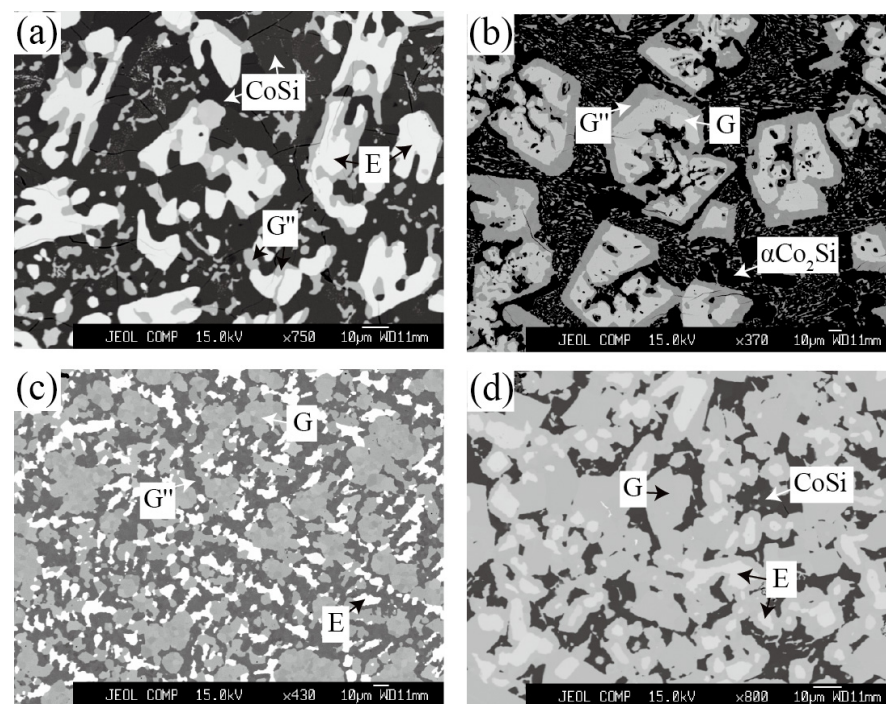


Figure 6. Typical ternary micrograph images obtained of (a) $\text{Co}_{46}\text{Ta}_{13}\text{Si}_{41}$ alloy annealed at $1100\text{ }^\circ\text{C}$ for 60 days; (b) $\text{Co}_{58}\text{Ta}_{10}\text{Si}_{32}$ alloy annealed at $1100\text{ }^\circ\text{C}$ for 60 days; (c) $\text{Co}_{48}\text{Ta}_{22}\text{Si}_{30}$ alloy annealed at $1100\text{ }^\circ\text{C}$ for 60 days and (d) $\text{Co}_{48}\text{Ta}_{22}\text{Si}_{30}$ alloy annealed at $900\text{ }^\circ\text{C}$ for 90 days.

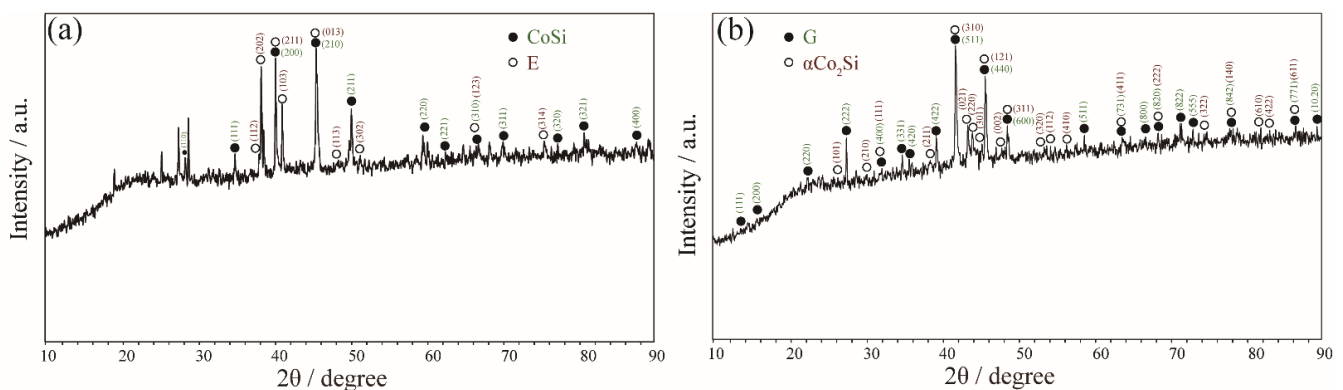


Figure 7. XRD patterns obtained of (a) $\text{Co}_{46}\text{Ta}_{13}\text{Si}_{41}$ alloy annealed at $1100\text{ }^\circ\text{C}$ for 60 days and (b) $\text{Co}_{58}\text{Ta}_{10}\text{Si}_{32}$ alloy annealed at $1100\text{ }^\circ\text{C}$ for 60 days.

3.1.4. Equilibria at Zone 4

Zone 4 describes the phase equilibria of other ternary phases including G and L. As shown in Figure 8a, the dark grey G phase was observed at the grain boundaries of the light grey λ_1 -Co₂Ta phase for the Co₅₄Ta₂₈Si₁₈ alloy after being annealed at 1100 °C. This morphology is extremely similar to that of the G phase precipitation on the C14 Laves phase [42].

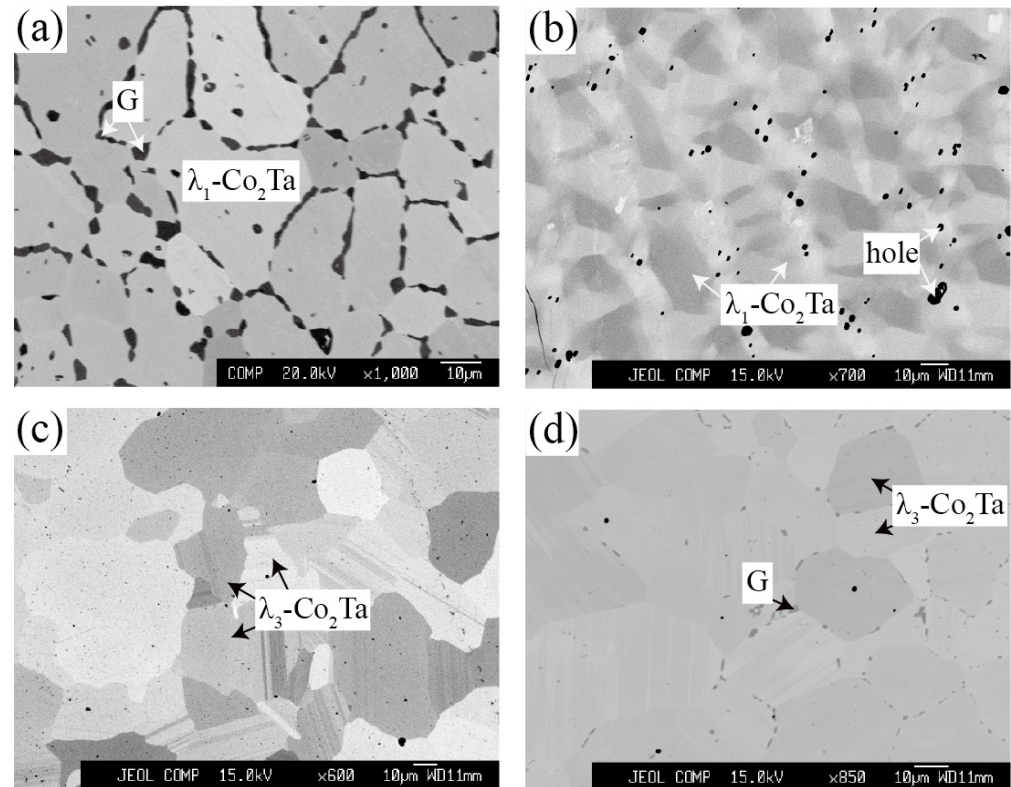


Figure 8. Typical ternary micrograph images obtained of (a) Co₅₄Ta₂₈Si₁₈ alloy annealed at 1100 °C for 60 days; (b) Co₅₉Ta₃₁Si₁₀ alloy annealed at 1100 °C for 60 days; (c) Co₆₅Ta₂₇Si₈ alloy annealed at 1100 °C for 60 days and (d) Co₆₅Ta₂₇Si₈ alloy annealed at 900 °C for 90 days.

The alloy with a nominal composition of Co₅₉Ta₃₁Si₁₀ was designed to detect the L phase as shown in Figure 8b. The interpretation of the corresponding XRD pattern in Figure 9a indicates that this ternary L phase crystallizes the same as the Zn₂Mg-type compounds (P6₃/mmc, C14) like the binary λ_1 -Co₂Ta phase. Additionally, the λ_1 -Co₂Ta phase is a high-temperature phase that only exists above 1294 °C [27]. However, the detected ternary L phase is stable at 900 °C and 1100 °C, suggesting that the addition of Si stabilizes the λ_1 -Co₂Ta phase toward low temperature. Besides, this Co-Ta-Si ternary L phase shows an extremely similar compositional range compared with the Ni-Nb-Si system [43]. The alloy Co₆₅Ta₂₇Si₈ was designed to determine the phase equilibria of the G and three Laves phases (λ_1 -Co₂Ta, λ_2 -Co₂Ta and λ_3 -Co₂Ta). A single λ_3 -Co₂Ta phase was detected in Co₆₅Ta₂₇Si₈ alloy annealed at 1100 °C (Figure 8c), while the λ_3 -Co₂Ta + G was observed for the same alloy being annealed at 900 °C (Figure 8d). The corresponding XRD patterns in Figure 9b,c confirm the above equilibrium relationship.

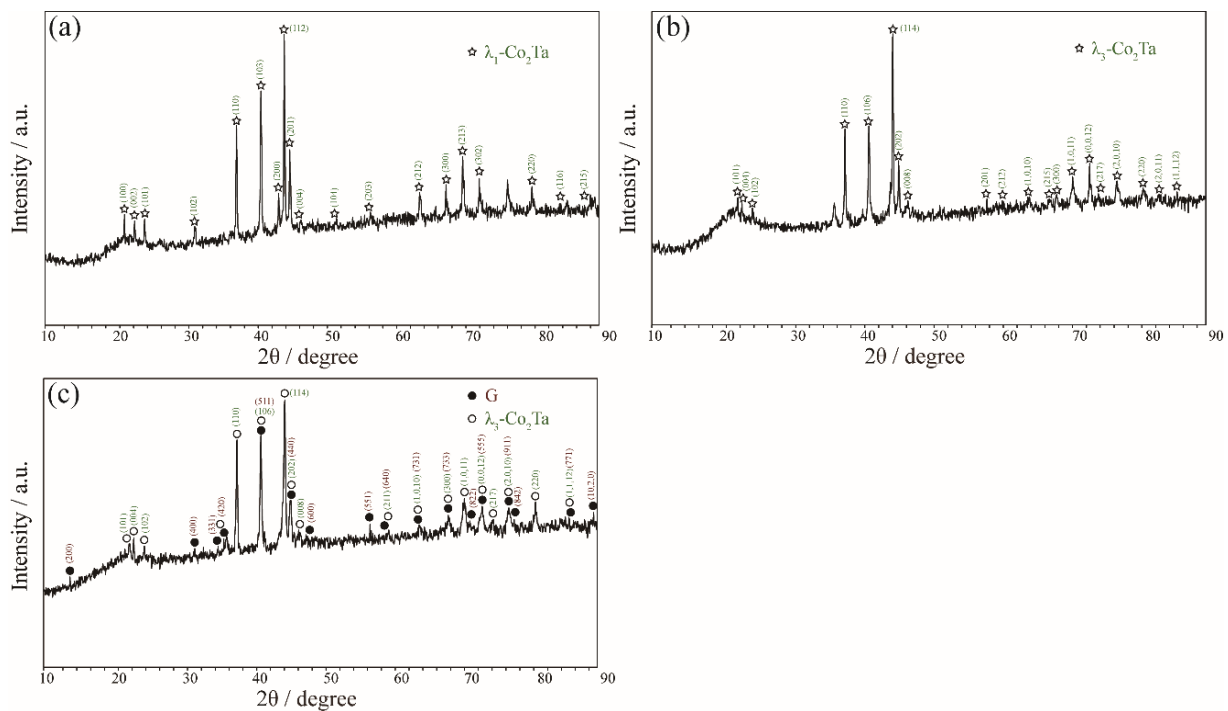


Figure 9. XRD patterns obtained of (a) $\text{Co}_{59}\text{Ta}_{31}\text{Si}_{10}$ alloy annealed at 1100 °C for 60 days; (b) $\text{Co}_{65}\text{Ta}_{27}\text{Si}_8$ alloy annealed at 1100 °C for 60 days and (c) $\text{Co}_{65}\text{Ta}_{27}\text{Si}_8$ alloy annealed at 900 °C for 90 days.

3.2. Isothermal Sections

Based on the phase equilibrium information discussed in Section 3.1, the isothermal sections of the Co-Ta-Si ternary system at 900 °C and 1100 °C are constructed in the whole composition range (see Figure 10). Nineteen and twenty-one three-phase regions were observed at 900 °C and 1100 °C, respectively. Few undetected three-phase regions are indicated by the dashed line.

The solid solubilities of Ta in the Co-Si binary phases (CoSi_2 , CoSi and $\alpha\text{Co}_2\text{Si}$) are negligible. The maximum solubility of Co in the TaSi_2 phase is 1.7 at.% at 1100 °C, and it increases to 3.4 at.% at 900 °C. When the temperature decreases from 1100 °C to 900 °C, the solid solubility of Co in the $\alpha\text{Ta}_5\text{Si}_3$ phase increases from 3.5 at.% to 5.3 at.%. In addition, the maximum solubility of Si in the $\lambda_3\text{-Co}_2\text{Ta}$ phase was measured to be 15.3 at.% at 1100 °C and decreased to 11.5 at.% at 900 °C. At least 8.5 at.% of Si can be dissolved in the $\lambda_2\text{-Co}_2\text{Ta}$ phase at 900 °C. However, the solid solubility of Si in Co_6Ta_7 hardly varies with temperature, maintaining 12 at.% at both 900 °C and 1100 °C.

In the Co-Ta-Si ternary system, there are four ternary compound phases G, G'' , E and V and a binary high-temperature phase $\lambda_1\text{-Co}_2\text{Ta}$ (L) stabilized by Si. The G, E, V and G'' phases are stoichiometric compounds exhibiting only small homogeneity ranges. Meanwhile, the G, E, V and L phases exist at 900 °C and 1100 °C. The G'' phase has also been reported in similar ternary systems like the Co-Nb-Si [41] and Co-Ti-Si [40]. The G'' phase was detected in the $\text{Co}_{46}\text{Ta}_{13}\text{Si}_{41}$, $\text{Co}_{58}\text{Ta}_{10}\text{Si}_{32}$ and $\text{Co}_{48}\text{Ta}_{22}\text{Si}_{30}$ alloys after being annealed at 1100 °C, but it disappears at 900 °C.

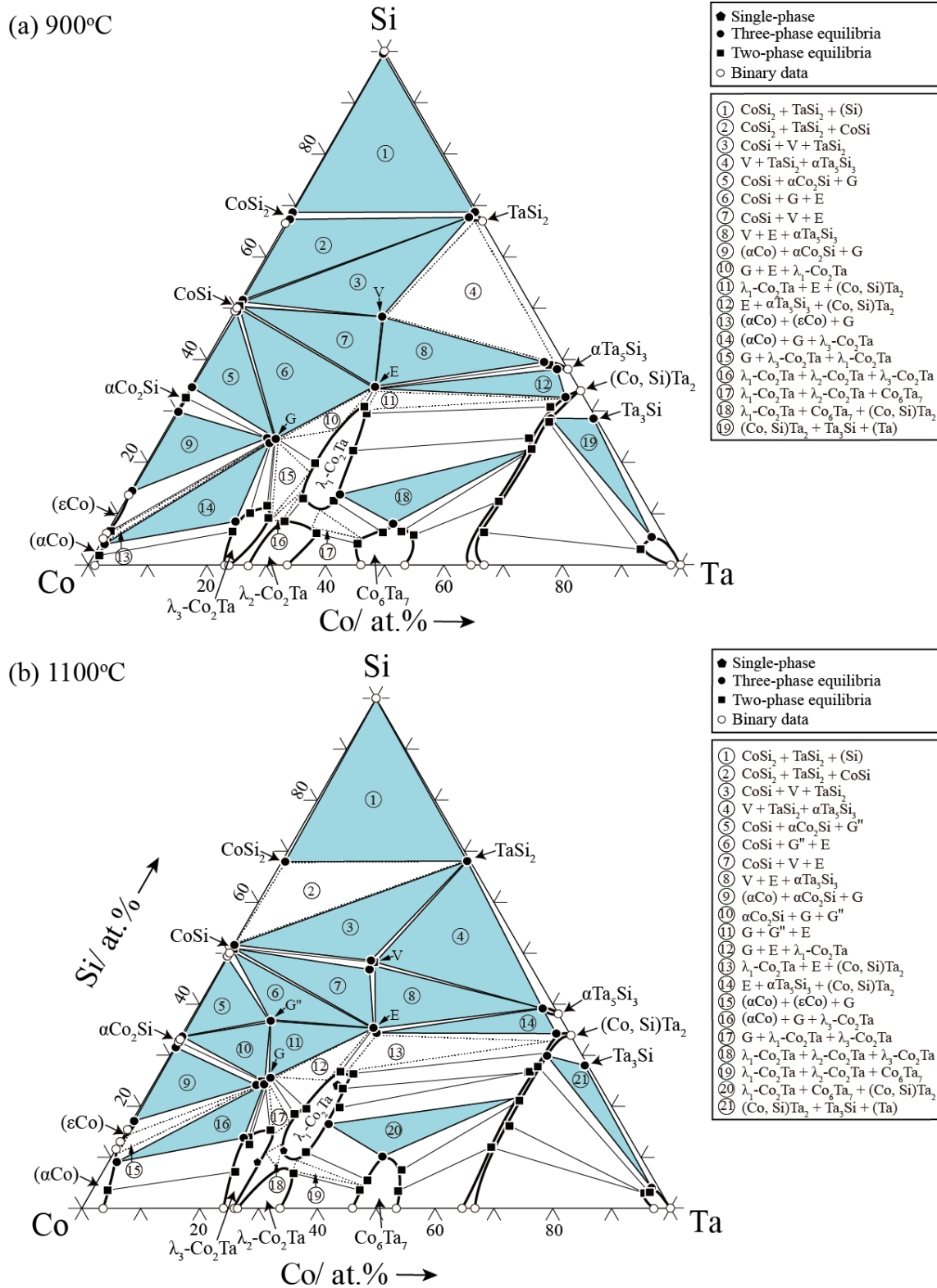


Figure 10. Experimental determined isothermal sections of the Co-Ta-Si system at (a) 900 °C and (b) 1100 °C.

4. Conclusions

The phase equilibrium of the Co-Ta-Si ternary system at 900 °C and 1100 °C is systematically studied by equilibrated alloy and the following conclusions can be drawn:

1. The four known ternary phases, G ($\text{Co}_{16}\text{Ta}_6\text{Si}_7$), E (CoTaSi), G'' (Co_4TaSi_3) and V ($\text{Co}_4\text{Ta}_4\text{Si}_7$) have almost no ternary solid solubilities, which could be treated as stoichiometric compounds.
2. The high-temperature phase G'' (Co_4TaSi_3) is only stable at 1100 °C and it disappears when the temperature decreases to 900 °C.
3. The addition of Si increases the thermal stability of the binary λ_1 -Co₂Ta (C14 Laves) phase, resulting in the formation of the ternary L phase with the composition of $\text{Co}_{32.3-58.8}\text{Ta}_{28.2-36.8}\text{Si}_{13.0-30.9}$ at 900 °C and $\text{Co}_{39.3-62.3}\text{Ta}_{26.8-33.9}\text{Si}_{10.9-26.8}$ at 1100 °C.
4. Both the binary CoTa₂ and SiTa₂ phases crystallize with the same body-centered tetragonal structure (space group: $I4/mcm$, C16) and they form a continuous solid solution phase (Co, Si)Ta₂.
5. The maximum solid solubility of Si for the λ_3 -Co₂Ta phase is ~15.3 at.% at 1100 °C and it slightly decreases to be ~11.5 at.% at 900 °C. The solid solubility of Si for the Co₆Ta₇ phase is always ~12 at.% and does not change with temperature.
6. The elemental Ta is hardly dissolved in the CoSi₂, CoSi and α -Co₂Si phases. Similarly, the elemental Co has negligible solubilities in the TaSi₂ and α -Ta₅Si₃ phases.

The results obtained from the present work make up the phase diagram information of the Co-Ta-Si ternary system, also provide the key experimental data for the establishment of Co-based superalloys thermodynamic database.

Author Contributions: Conceptualization, C.W. and X.L.; data curation, L.H. and P.Y., methodology, C.W., X.L. and M.Y.; investigation, X.H., L.H. and J.Z.; writing—original draft preparation, X.H. and L.H.; writing—review and editing, L.H., M.Y., Y.C., S.Y. and J.Z.; supervision, C.W. and X.L.; funding acquisition, C.W., M.Y. and X.L. All authors have read and agreed to the published version of the manuscript.

Funding: This research was funded by the National Nature Science Foundation of China, grant number 51971082, 51831007 and the National Post-doctoral Program for Innovative Talents, grant number BX20200103.

Institutional Review Board Statement: Not applicable.

Informed Consent Statement: Not applicable.

Data Availability Statement: Data sharing not applicable.

Conflicts of Interest: The authors declare no conflict of interest.

References

1. Sato, J.; Omori, T.; Oikawa, K.; Ohnuma, I.; Kainuma, R.; Ishida, K. Cobalt-Base High-Temperature Alloys. *Science* **2006**, *312*, 90. [[CrossRef](#)] [[PubMed](#)]
2. Mitrica, D.; Badea, I.C.; Serban, B.A.; Olaru, M.T.; Vonica, D.; Burada, M.; Piticescu, R.-R.; Popov, V.V. Complex Concentrated Alloys for Substitution of Critical Raw Materials in Applications for Extreme Conditions. *Materials* **2021**, *14*, 1197. [[CrossRef](#)]
3. Bocchini, P.J.; Sudbrack, C.K.; Noebe, R.D.; Dunand, D.C.; Seidman, D.N. Effects of titanium substitutions for aluminum and tungsten in Co-10Ni-9Al-9W (at %) superalloys. *Mater. Sci. Eng. A* **2017**, *705*, 122–132. [[CrossRef](#)]
4. Reyes Tirado, F.L.; Perrin Toinin, J.; Dunand, D.C. $\gamma + \gamma'$ microstructures in the Co-Ta-V and Co-Nb-V ternary systems. *Acta Mater.* **2018**, *151*, 137–148. [[CrossRef](#)]
5. Berthod, P.; Ozouaki, S.; Aranda, L.; Medjahdi, G.; Etienne, E. Kinetic and Metallography Study of the Oxidation at 1250 °C of {Co + Ni}-Based Superalloys Containing Ti to Form MC Carbides. *Metals* **2022**, *12*, 10.
6. Xu, W.; Wang, Y.; Wang, C.; Liu, X.; Liu, Z.-K. Alloying effects of Ta on the mechanical properties of γ' Co₃(Al, W): A first-principles study. *Scr. Mater.* **2015**, *100*, 5–8. [[CrossRef](#)]
7. Yan, H.; Vorontsov, V.; Dye, D. Effect of alloying on the oxidation behaviour of Co–Al–W superalloys. *Corros. Sci.* **2014**, *83*, 382–395. [[CrossRef](#)]
8. Klein, L.; Shen, Y.; Killian, M.S.; Virtanen, S. Effect of B and Cr on the high temperature oxidation behaviour of novel γ/γ' -strengthened Co-base superalloys. *Corros. Sci.* **2011**, *53*, 2713–2720. [[CrossRef](#)]

9. Zhu, L.; Wei, C.; Qi, H.; Jiang, L.; Jin, Z.; Zhao, J.-C. Experimental investigation of phase equilibria in the Co-rich part of the Co-Al-X (X = W, Mo, Nb, Ni, Ta) ternary systems using diffusion multiples. *J. Alloys Compd.* **2017**, *691*, 110–118. [[CrossRef](#)]
10. Yeh, A.; Wang, S.; Cheng, C.; Chang, Y.; Chang, S. Oxidation Behaviour of Si-Bearing Co-Based Alloys. *Oxid. Met.* **2016**, *86*, 99–112. [[CrossRef](#)]
11. Liang, Z.; Göken, M.; Lorenz, U.; Neumeier, S.; Oehring, M.; Pyczak, F.; Stark, A.; Wang, L. Influence of small amounts of Si and Cr on the high temperature oxidation behavior of novel cobalt base superalloys. *Corros. Sci.* **2021**, *184*, 109388. [[CrossRef](#)]
12. Wang, C.; Zhang, C.; Wang, Y.; Han, J.; Xu, W.; Liu, X. Effects of Transition Elements on the Structural, Elastic Properties and Relative Phase Stability of L12 γ' -Co₃Nb from First-Principles Calculations. *Metals* **2021**, *11*, 933. [[CrossRef](#)]
13. Lass, E.A. The effects of Fe and Si on the phase equilibria in a γ' -strengthened Co–Al–W-based superalloy. *J. Alloys Compd.* **2020**, *825*, 154158. [[CrossRef](#)]
14. Noubary, K.D.; Kellner, M.; Nestler, B. Rotating Directional Solidification of Ternary Eutectic Microstructures in Bi-In-Sn: A Phase-Field Study. *Materials* **2022**, *15*, 1160. [[CrossRef](#)]
15. Yang, X.; Zhang, L.; Sobolev, S.; Du, Y. Kinetic phase diagrams of ternary Al-Cu-Li system during rapid solidification: A phase-field study. *Materials* **2018**, *11*, 260. [[CrossRef](#)]
16. Yang, T.; He, W.; Chen, G.; Zeng, W.; Wang, J.; Zeng, L.; Liang, J. The Phase Relations of the Co-Ni-In Ternary System at 673 K and 873 K and Magnetic Properties of Their Compounds. *Materials* **2020**, *13*, 3990. [[CrossRef](#)]
17. Ledwig, P.; Kac, M.; Kopia, A.; Falkus, J.; Dubiel, B. Microstructure and Properties of Electrodeposited Nanocrystalline Ni-Co-Fe Coatings. *Materials* **2021**, *14*, 3886. [[CrossRef](#)]
18. Yuan, Z.; Kobayashi, S. Determination of Phase Equilibria among δ -Fe, γ -Fe and Fe₂M Phases in Fe-Cr-M (M: Hf, Ta) Ternary Systems. *Metals* **2022**, *12*, 102. [[CrossRef](#)]
19. Strutynski, C.; Evrard, M.; Le Gendre, A.; Maldonado, A.; Désévéday, F.; Gadret, G.; Jules, J.-C.; Smektala, F. Physicochemical Properties and Fiber-Drawing Ability of Tellurite Glasses in the TeO₂-ZnO-Y₂O₃ Ternary System. *Materials* **2022**, *15*, 1177. [[CrossRef](#)]
20. Uchida, Y.; Watanabe, C.; Tsuruoka, H. Basic Evaluation of Phase Relation in a Phosphorus-Containing System Saturated with CaSiO₃ at Elevated Temperatures for the Utilization of Steelmaking Slag and Sewage Sludge as Phosphorus Resources. *Minerals* **2022**, *12*, 266. [[CrossRef](#)]
21. Barauskaite, V.; Belysheva, M.; Pestova, O.; Anufrikov, Y.; Skripkin, M.; Kondratiev, Y.; Khripun, V. Thermodynamic Description of Dilution and Dissolution Processes in the MgCl₂-CsCl-H₂O Ternary System. *Materials* **2021**, *14*, 4047. [[CrossRef](#)] [[PubMed](#)]
22. Chen, Y.; Wang, C.; Ruan, J.; Yang, S.; Omori, T.; Kainuma, R.; Ishida, K.; Han, J.; Lu, Y.; Liu, X. Development of low-density γ/γ' Co-Al-Ta-based superalloys with high solvus temperature. *Acta Mater.* **2020**, *188*, 652–664. [[CrossRef](#)]
23. Chen, Y.; Wang, C.; Ruan, J.; Omori, T.; Kainuma, R.; Ishida, K.; Liu, X. High-strength Co–Al–V-base superalloys strengthened by γ' -Co₃ (Al, V) with high solvus temperature. *Acta Mater.* **2019**, *170*, 62–74. [[CrossRef](#)]
24. Volz, N.; Xue, F.; Zenk, C.H.; Bezold, A.; Gabel, S.; Subramanyam, A.; Drautz, R.; Hammerschmidt, T.; Makineni, S.K.; Gault, B. Understanding creep of a single-crystalline Co-Al-W-Ta superalloy by studying the deformation mechanism, segregation tendency and stacking fault energy. *Acta Mater.* **2021**, *214*, 117019. [[CrossRef](#)]
25. Lenz, M.; Wu, M.; Spiecker, E. Segregation-assisted climb of Frank partial dislocations: An alternative route to superintrinsic stacking faults in L12-hardened superalloys. *Acta Mater.* **2020**, *191*, 270–279. [[CrossRef](#)]
26. Zhang, L.; Du, Y.; Xu, H.; Pan, Z. Experimental investigation and thermodynamic description of the Co–Si system. *Calphad* **2006**, *30*, 470–481. [[CrossRef](#)]
27. Zhou, C.; Guo, C.; Li, C.; Du, Z. Thermodynamic description of the Co–Ni–Ta system. *Calphad* **2019**, *66*, 101649. [[CrossRef](#)]
28. Drouelle, I.; Servant, C. Thermodynamic assessment of the Si–Ta system. *J. Alloys Compd.* **2013**, *551*, 293–299. [[CrossRef](#)]
29. Beck, F. Ternary G and E silicides and germanides of transition elements. *Trans. Met. Soc. AIME* **1963**, *27*, 575.
30. Vilasi, M.; Venturini, G.; Steinmetz, J.; Malaman, B. Structure of “TaCo₄Si₃”, a new silicide closely related to the Y13Pd₄₀Sn₃₁ stannide. *J. Alloys Compd.* **1995**, *227*, 32–36. [[CrossRef](#)]
31. Gladyshevsky, E. New ternary compounds with a structure of the Mg₆Cu₁₆Si₇ type. *Dopov. Akad. Nauk Ukr. SSR* **1962**, *4*, 481–483.
32. Trojko, R.; Blažina, Ž. Metal-metalloid exchange in some Friauf-Laves phases containing two transition metals. *J. Less-Common. Met.* **1985**, *106*, 293–300. [[CrossRef](#)]
33. Mittal, R. Si-Stabilised C14 laves phases in the transition metal systems. *J. Less-Common. Met.* **1978**, *60*, 75–82. [[CrossRef](#)]
34. Jeitschko, W.; Jordan, A.; Beck, P. V and E phase in ternary systems with transition metals and silicon or germanium. *Trans. Met. Soc. AIME* **1969**, *245*, 335–339.
35. Markiv, V. The crystal structures of the compounds R (M, X)₂ and RMX₂ in Zr-Ni-Al, Ti-Fe-Si and related systems. *Acta Cryst.* **1966**, *21*, 84–85.
36. Markiv, B.; Gladyshevskii, E.; Skolozdra, R.; Krypyakevich, P. Ternary compounds RX₂ in the systems Ti–V (Fe, Co, Ni)–Si and some related systems. *Dopovidi Akad. Nauk. Ukr. Koi RSR SERIYA A Fiz.-Tekhnichni Ta Mat. Nauk.* **1967**, *3*, 266–269.
37. Beattie, H.J.; Versnyder, F.L. A New Complex Phase in a High-Temperature Alloy. *Nature* **1956**, *178*, 208–209. [[CrossRef](#)]
38. Yan, X.; Grytsiv, A.; Rogl, P.; Pomjakushin, V.; Xue, X. On the crystal structure of the Mn–Ni–Si G-phase. *J. Alloys Compd.* **2009**, *469*, 152–155. [[CrossRef](#)]
39. Matsukawa, Y.; Takeuchi, T.; Kakubo, Y.; Suzudo, T.; Watanabe, H.; Abe, H.; Toyama, T.; Nagai, Y. The two-step nucleation of G-phase in ferrite. *Acta Mater.* **2016**, *116*, 104–113. [[CrossRef](#)]

40. Hu, X. The 1100 °C Isothermal Section of the Ti-Co-Si Ternary System. *J. Phase Equilibria* **2001**, *22*, 114–121. [[CrossRef](#)]
41. Gupta, K. The Co-Nb-Si (Cobalt-Niobium-Silicon) System. *J. Phase Equilibria Diffus.* **2010**, *31*, 308–312. [[CrossRef](#)]
42. Wang, C.; Huang, L.; Yang, M.; Huang, X.; Zhang, J.; Pan, S.; Yang, S.; Liu, X. Experimental investigation of phase equilibria in the Ni-Ta-Si refractory alloy system. *J. Alloys Compd.* **2021**, *888*, 161467. [[CrossRef](#)]
43. Santos, V.; Eleno, L.; Schön, C.; Richter, K. Experimental investigation of phase equilibria in the Nb–Ni–Si refractory alloy system at 1323 K. *J. Alloys Compd.* **2020**, *842*, 155373. [[CrossRef](#)]